UNIVERSITY OF OKLAHOMA

GRADUATE COLLEGE

# Searching for Supersymmetric Particles at the Large Hadron Collider using the ATLAS Detector

A DISSERTATION

SUBMITTED TO THE GRADUATE FACULTY

in partial fulfillment of the requirements for the

Degree of

DOCTOR OF PHILOSOPHY

By

OTHMANE RIFKI
Norman, Oklahoma
2016

Searching for Supersymmetric Particles at the Large Hadron Collider using the ATLAS Detector

A DISSERTATION APPROVED FOR THE
HOMER L. DODGE DEPARTMENT OF PHYSICS AND
ASTRONOMY

BY

Dr. Brad Abbott, Chair

Dr. Peter Parker, Outside Member

Dr. Mike Strauss

Dr. Chung Kao

Dr. Eric Abraham

To my loving parents and sister.

# Acknowledgements

I would like to acknowledge...

# Table of Contents

# Abstract

Well now this is my abstract.

# Preface

...

In the spring of 2014, I received an ATLAS Support Center graduate fellowship to move to Argonne National Laboratory to work on hardware and physics analysis. This thesis is based on the work conducted in the period of May 2014 to May 2017. In my research, the supervision of Dr. Brad Abbott has been invaluable.

There is a very long list of people I would like to thank. I would like to thank the Argonne group for the warm welcome to the physics division at Argonne. The scientits at Argonne became colleagues and friends.

The working conditions either in Oklahoma, Argonne, or CERN have been excellent. I had the privileage of interacting with many interesting people at these institutes which I contributed significantly to building my independence as a physicist. I habe been particularly fortunate of being part of Argonne National Laboratory. where I am able to work with many talented physicsits. I would like to start with Alexander Paramonov and Sergei Chekanov who were the first to introduce me to physics analysi. Robert Blair, Jeremy Love, and Jinlong Zhang with whom I evolved the glorious region of interest builder of ATLAS responsible for processing every event recorded by the ATLAS detector. It was a real joy working with them and bringing the project to completion and taking data in ATLAS. It is fair to say that James Proudfoot became a mentor to me during my stay at Argonne and afterwards. Furthermore, my gratitude goes to Ximo Poveda, Julien Maurer, and Otilia Ducu who made my work within the same sign

SUSY group a real joy.

Finally, I would like to thank my family and frineds for their support and acceptance of my absence from their lives. Last, but not least, I thank ... encouragement and patience during these years.

Othmane Rifki, May 2017

# Introduction

Chapter 1

# Theoretical Background

Chapter 2

# The LHC and the ATLAS Experiment

Chapter 3

# The Region of Interest Builder

Chapter 4

# Object Reconstruction

# Chapter 5

# Data-driven techniques to estimate fake lepton backgrounds

## 5.1 The problem of fakes

The reconstructed objects (leptons, photons, $b$-jets, etc.) in a collision event are used to perform a wide range of SM measurements or searches for evidence of BSM physics. The assumption is that these objects are 'real' representing the desired particles in the final state used in the analysis. In practice, the reconstructed objects might not be always 'real'. In fact, they may be something completely different that was mistakenly reconstructed as the desired object, called 'fake'. For the purpose of the analysis presented in this thesis, the focus is on 'fake' leptons. To illustrate the problem, a hadronic jet may deposit more energy in the electromagnetic calorimeter than the hadronic calorimeter, or that it leaves a narrow deposit of energy leading the reconstruction alogorithms to mistake this jet for an electron. From the analysis point of view, the 'fake' electron will pass all the selection criteria and will be indistinguishable from a 'real' electron. It is important for the analysis that requires a reconstructed electron to model the fake electron background to get a sound result. This example was given with electrons, but can be generalized to muons as well. In short, any analysis that uses leptons in the final state must account for the 'fake' lepton background. This background can be more or less important depending on the detector, the analysis selection,

and the number of leptons required. To estimate this background it is important to first understand what type of processes lead to fake leptons.

## 5.2 Common processes for faking leptons

The reconstruction of 'fake' leptons can be an instrumental effect related to the inability to identify the object based on its measured properties by the detector. In this case, the reconstructed lepton is not a real lepton and the production process will be different for electrons and muons.

The reconstruction of electrons relies on the observation of well aligned particle hits in the layers of the ID that are consistent with an energy deposition in the EM calorimeter. Photons can mimick this signature since they deposit energy in the EM calorimeter that happens to be alligned with a charged track. A jet for example containing charged and neutral pions can lead to such scenarios. It is possible for the jet to have one charged pion leaving a track similar to that of an electron. The decay of $\pi^0$ mesons to photons in this jet can deposit energy in the EM calorimeter leading to the required signature. Another mechanism that can lead to fake electrons is the emission of photons via Brehmstrahlung from high energy muons. The muon track can be mistaken for that of an electron and the photons interact with the EM calorimeter leading to a signature similar to that of electrons. An additional process is that of photon conversions into a $e^+e^-$.

The reconstruction of muons relies on the observation of tracks from the ID matched to tracks from the muon spectrometer. It is possible for charged hadrons

with long lifetime to traverse the calorimeter layers and leave hits in the muon spectrometer. These hits may coincide with other hits from the ID due to the random activity in the event. As a result, a muon can get reconstructed. Another instance may occur when pions or kaons decay in-flight to muons in the muon spectrometer and happen to align with the primary vertex.

The leptons that are used in the physics analyses must be coming from the hard scatter, generally referred to as prompt leptons. There is another case where the reconstructed lepton is a real lepton but is not a lepton coming from the hard interaction, referred to as non-prompt leptons. Non-prompt leptons can be produced from heavy flavor meson decays with a low energy activity around the lepton which allows it to pass isolation requirements. A good example of this type of process is the semi-leptonic decay of top quark pair which contribute to final states with two leptons.

For the rest of the thesis, the fake leptons will be referred to as fake/non-prompt (FNP) leptons. There are several methods used to perform the estimation of FNP lepton backgrounds. A method that the author developed will be described next along with a standard method for estimating this type of backgrounds. The benefit of having two methods for estimating the FNP lepton background is to have enough confidence in the final estimate. The two methods use different assumptions which naturally leads to a more robust estimation of this difficult background. Moreover, the final estimate of the FNP lepton background is taken as a statistical combination of the estimates from the two methods leading to a reduction of the systematic uncertainties on the estimate.

## 5.3 Monte Carlo Template Method

### 5.3.1 Motivation

The processes leading to FNP leptons depend on the selection applied in the analysis. For instance, a selection with same-sign leptons will have contributions from top quark pair production ($t\bar{t}$) or the associated production of a vector boson and jets ($W$+jets or $Z$+jets).These processes cannot give two leptons of the same electric charge unless there is a charge mis-measurement (mainly affecting electrons) or that a FNP lepton was produced. It is possible to generate the processes that can contribute to a FNP lepton, such as $t\bar{t}$ or $V$+jets, with Monte Carlo event generators processed through Geant4 detector simulation of the ATLAS detector. This approach will yield an estimate however it might not be reliable. For instance, the detector simulation itself might not reproduce the true behavior of the interaction of the physics objects with the detector, particularly when looking at rare processes such as the production of FNP leptons. The second limitation is in the generation of enough MC events to probe the region of the phase space targetted by the analysis which affects the statistical uncertainties in the estimates. The latter concern is addressed by ensuring that the simulations for the major backgrounds ($t\bar{t}$ and $V$+jets) have much higher event count than the corresponding number of events observed in the data sample. In fact, these backgrounds have a large number of simulated events because they are important for many analyses (including SM measurements and BSM searches). The rest of the section will concentrate on addressing the former limitation.

### 5.3.2 Description of the method

The MC template method relies on the correct modelling of FNP leptons kinematics in MC simulation to extrapolate background predictions from control regions to the signal regions. The method assumes that the kinematic shapes for each source of FNP lepton is correctly modeled in the simulations, and the normalization for each source is extracted in a combined fit to data control regions. The number of normalization factors depend on the number of identified origins of the FNP lepton in the signal regions and the control regions are designed to constrain these factors in regions enriched with FNP leptons from the same origin.

To illustrate the approach, we describe the application of the method in SS/3L analysis later described in this thesis. The processes of interest that may lead to a FNP lepton or a charge flip are $t\bar{t}$ and $V$+jets. FNP leptons are classified using an algorithm that navigates the generator particle record to determine where the FNP lepton is originating from. The lepton is classified as either an electron or a muon that is prompt from decays of on-shell $W$ and $Z$ bosons, non-prompt from a heavy flavor $b$ decay (HF), or fake from mis-identification of a light flavor jet or a photon (LF). In the case of an electron, we further classify the prompt electrons to prompt electrons with the correct charge or with a charge mis-measurement, commonly named charge flip. In total, five categories referred to as MC templates are construced following the classification illustarted in figure 5.1.

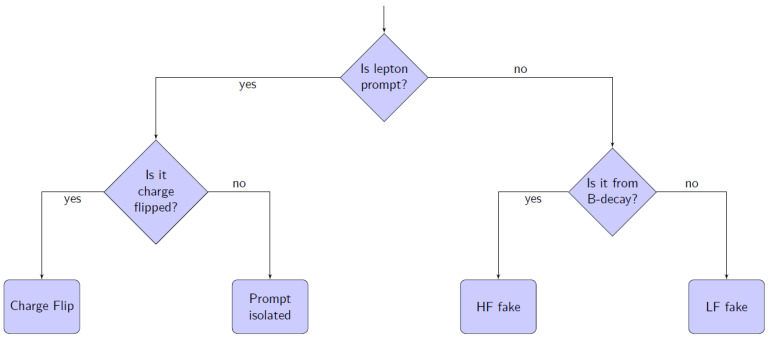


Figure 5.1: Lepton classification.

### 5.3.3 Correction factors

The FNP estimate relies on kinematic extrapolation using processes expected to contribute via FNP leptons from control regions with low jet multiplicity and $E_{\mathrm{T}}^{\mathrm{miss}}$, to the signal regions that require high jet multiplicity and $E_{\mathrm{T}}^{\mathrm{miss}}$. The control regions are chosen to separate FNP leptons from HF origins and FNP leptons from LF origins. For instance, a control sample characterized by the presence of a $b$-jet will be enriched in processes with one FNP lepton that is coming from a HF decay, while a sample characterized by the absence of a $b$-jet will have one FNP lepton from LF decay. The presence of one FNP lepton in the control sample allows the correction of the production rate of these FNP leptons by performing a fit to data.

For example, if a Z$\rightarrow \mu\mu$+LF jet event is reconstructed as a $\mu^+\mu^-e^+$ event, then the electron is fake. Therefore, a correction of LF jet $\rightarrow$ e (Fr(LF$\rightarrow$e)) is applied to the rate of $\mu\mu e$ events. The correction Fr(LF$\rightarrow$e) is constrained by a fit to data in control regions dominated by LF jet $\rightarrow$ e type fakes. Similarly, three other corrections are defined as LF jet $\rightarrow \mu$ (Fr(LF$\rightarrow \mu$)), HF jet $\rightarrow$ e

(Fr(HF→e)), HF jet → $\mu$ (Fr(HF→ $\mu$)). An additional correction is applied to correct the charge flip rate predicted by simulation. For example, a Z→ $e^+e^-$ event is reconstructed as $e^+e^+$ or $e^-e^-$. The simulation takes into account the charge flip rate but it might be off. The charge flip (Cf(e)) correction derived from a data fit is expected to recover this mis-modeling. The charge flip rate only concern electrons as the muon charge flip rate is negligeable.

A likelihood fit is defined as the product of the Poisson probabilities describing the observed events in the binned distributions from the expected number of events rescaled by the five multipliers which are left free to float in the fit. These multipliers are applied to the MC predictions in the signal regions to obtain an estimation of the charge flip and FNP backgrounds.

### 5.3.4 Control regions

The corrections depend on the simulated sample, the reconstructed final state, and the flavor of the leptons. As a result, care must be taken when designing the control regions used to perform the fit of the FNP leptons and electron charge flip templates. For instance, each template needs to be constrained in a selection that is representative of the processes leading to FNP leptons and charge flip electrons present in the kinematic region targetted by the search for BSM physics.

In the SS/3L analysis discussed in this thesis the control regions are defined with at least two same-sign leptons, $E_{\mathrm{T}}^{\mathrm{miss}} > 40$ GeV, two or more jets. This preselection ensures that the FNP leptons are not from fakes originating from QCD like event topologies. They are further split in regions with or without

$b$-jets to constrain the HF and LF leptons respectively. In addition, they are also split with different flavours of the same-sign lepton pair ee, e$\mu$, and $\mu\mu$, giving a total of six control regions. Any event entering the signal region is vetoed. The ee channel will constrain the charge flip correction factor, fake leptons from LF decays in the selection without $b$-jets, and non-prompt decay from HF in the selection with $b$-jets. The $\mu\mu$ channel will constrain the muon fake rates in the LF and HF decays for the selection without or with $b$-jets, respectively. The e$\mu$ channel will constrain both the electron and muon fakes for events containing both lepton flavors.

The six distributions are chosen for variables that provide the best separation between processes with prompt leptons and processes with FNP leptons and charge flip and are shown before and after the fit in Figures 5.2-5.4 and Figures 5.3-5.5, respectively.

The minimization of the negative log likelihood using the MINUIT package leads to the multipliers shown in Tables 5.1 and 5.2. The tables represent the multipliers obtained from the fit upon using two different parton showers, POWHEG-BOX and SHERPA for the processes that lead to FNP leptons and charge flips. The systematic uncertainty is obtained by varying the generator from POWHEG-BOX to SHERPA and evaluating the impact on the expected background from FNP and charge flip leptons. It is found to be the dominant contribution to the systematic uncertainty of the method (up to 80%). The uncertainties in the multipliers themselves correspond to how much the parameter needs to be varied for a one standard deviation change in the likelihood function. This uncertainty takes into

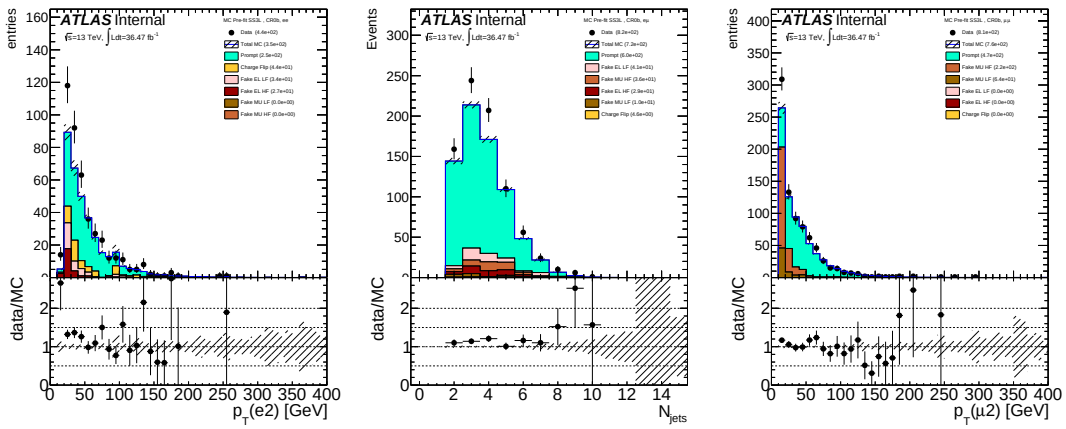


Figure 5.2: Pre-fit distributions for $ee$ channel (left), for $e\mu$ channel (middle), and for $\mu\mu$ channel (right) from CR0b that were used in the fit to extract the FNP lepton and charge flip multipliers. The generator used in these plots is Powheg. The hashed band represents the sum of systematic uncertainties on the predictions.

account the limited number of simulated events and is included as a systematic uncertainty on the expected number of background events.

## 5.4 Matrix Method

The FNP leptons do not often pass one of the lepton selection criteria but have non-zero impact parameter, and are often not well-isolated. These selection requirements are key ingredients to control the FNP leptons. The number of events with at least one FNP lepton is estimated using two classes of leptons: a real-enriched class of "tight" leptons corresponding to signal leptons and a fake-enriched class of "loose" leptons corresponding to candidate leptons with

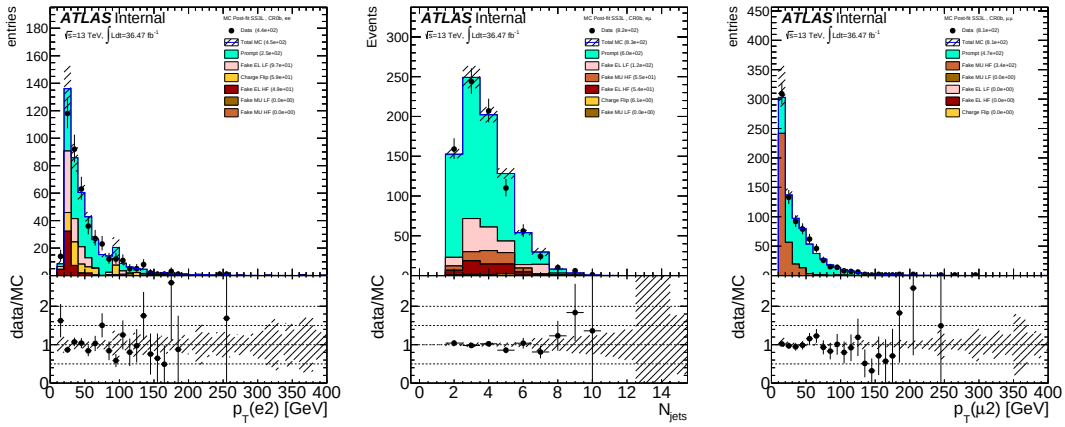


Figure 5.3: Post-fit distributions for $ee$ channel (left), for $e\mu$ channel (middle), and for $\mu\mu$ channel (right) from CR0b that were used in the fit to extract the FNP lepton and charge flip multipliers. The generator used in these plots is Powheg. The hashed band represents the sum of systematic uncertainties on the predictions.

Table 5.1: The FNP and charge flip multipliers obtained after minimizing the likelihood function using Pythia. The uncertainty in the multipliers takes into account the limited statistics of simulated events.

| Category | Multiplier | Uncertainty |
|---|---|---|
| chFlip | 1.49 | 0.58 |
| HF EL | 2.80 | 0.98 |
| LF EL | 2.89 | 0.88 |
| HF MU | 1.59 | 0.31 |
| LF MU | 1.00 | 1.34 |

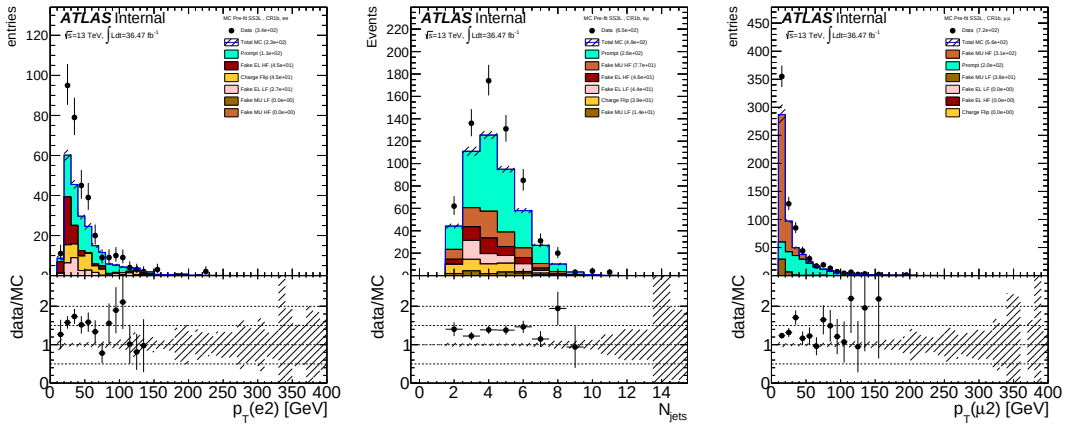


Figure 5.4: Pre-fit distributions for $ee$ channel (left), for $e\mu$ channel (middle), and for $\mu\mu$ channel (right) from CR1b that were used in the fit to extract the FNP lepton and charge flip multipliers. The generator used in these plots is Powheg. The hashed band represents the sum of systematic uncertainties on the predictions.

Table 5.2: The FNP and charge flip multipliers obtained after minimizing the likelihood function using Sherpa. The uncertainty in the multipliers takes into account the limited statistics of simulated events.

| Category | Multiplier | Uncertainty |
|---|---|---|
| chFlip | 1.34 | 0.58 |
| HF EL | 2.40 | 0.85 |
| LF EL | 1.83 | 1.04 |
| HF MU | 1.17 | 0.16 |
| LF MU | 2.40 | 0.81 |

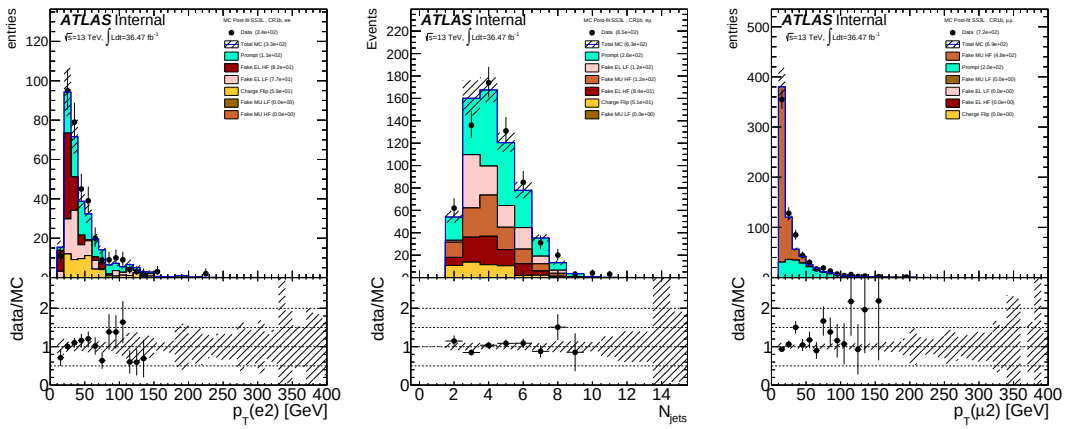


Figure 5.5: Post-fit distributions for $ee$ channel (left), for $e\mu$ channel (middle), and for $\mu\mu$ channel (right) from CR1b that were used in the fit to extract the FNP lepton and charge flip multipliers. The generator used in these plots is Powheg. The hashed band represents the sum of systematic uncertainties on the predictions.

relaxed identification criteria[1]. In the next sections, a description of the simplest form of the matrix method will be given with events containing one object. Then a generalized treatment that can handle events with an arbitrary number of leptons in the final states will be discussed.

### 5.4.1 Events with one object

Given the probabilities $\varepsilon/\zeta$ for a real/FNP candidate lepton to satisfy the signal lepton criteria, one can relate the number of events with one candidate lepton passing/failing signal requirements ($n_{\text{pass}}/n_{\text{fail}}$) to the number of events with one real/FNP signal leptons ($n_{\text{real}}/n_{\text{FNP}}$):

[1]Signal leptons are leptons satisfying the signal lepton definition, while the candidate leptons are leptons satisfying some pre-selection cuts and usually passing the overlap removal requirements as discssed in the analysis section ??.

$$\begin{pmatrix} n_{\text{pass}} \\ n_{\text{fail}} \end{pmatrix} = \begin{pmatrix} \varepsilon & \zeta \\ 1-\varepsilon & 1-\zeta \end{pmatrix} \begin{pmatrix} n_{\text{real}} \\ n_{\text{FNP}} \end{pmatrix}; \tag{5.1}$$

allowing to determine the unknown number of events $n_{\text{FNP}}$ from the observed $n_{\text{pass}}$ and $n_{\text{fail}}$ given measurements of the probabilities $\varepsilon/\zeta$.

The predictive power of the matrix method comes from the fact that the real and FNP leptons have different composition in the two collections of tight and loose objets leading to $\varepsilon \neq \zeta$. In fact, the tight lepton collection will be dominated by real objects while the loose region will be dominated by fake objects. As a result, the inequality $\varepsilon >> \zeta$ will always hold true which guarantees that the martrix in Eq. 5.1 is invertible and gives positive estimates.

The next step is to invert the relation in Eq. 5.1 to obtain

$$\begin{pmatrix} n_{\text{real}} \\ n_{\text{FNP}} \end{pmatrix} = \frac{1}{\varepsilon - \zeta} \begin{pmatrix} \bar{\zeta} & -\zeta \\ -\bar{\varepsilon} & \varepsilon \end{pmatrix} \begin{pmatrix} n_{\text{pass}} \\ n_{\text{fail}} \end{pmatrix}; \tag{5.2}$$

where $\bar{\varepsilon} = 1 - \varepsilon$ and $\bar{\zeta} = 1 - \zeta$. The FNP lepton component is:

$$n_{\text{FNP}} = \frac{1}{\varepsilon - \zeta} \left( (\varepsilon - 1)\, n_{\text{pass}} + n_{\text{fail}} \right). \tag{5.3}$$

However, the quantity of interest is the expected FNP lepton background that passes the tight selection criteria: $n_{\text{pass} \cap \text{FNP}} = \zeta n_{\text{FNP}}$. To obtain this quantity, the identity from Eq. 5.1 is used to get:

$$n_{\text{FNP}} = \frac{\zeta}{\varepsilon - \zeta} \left( (\varepsilon - 1)\, n_{\text{pass}} + n_{\text{fail}} \right). \tag{5.4}$$

The linearity of Eq. 5.4 with respect to $n_{\text{pass}}$ and $n_{\text{fail}}$ allows the method to be applied on an event-by-event, effectively resulting into a weight being assigned to each event. By defining

$$n_{\text{pass}} = \sum_{\text{all events}} \mathbb{1}_{\text{pass}},\ n_{\text{fail}} = \sum_{\text{all events}} \mathbb{1}_{\text{fail}},\ \mathbb{1}_{\text{fail}} = 1 - \mathbb{1}_{\text{pass}},$$

where $\mathbb{1}_{\text{pass(fail)}} = 1$ if the object pass (fail) the tight selection requirement and $\mathbb{1}_{\text{pass(fail)}} = 0$ otherwise. Eq. 5.4 can be written as

$$n_{\text{FNP}} = \sum_{\text{all events}} \{\frac{\zeta}{\varepsilon - \zeta}(\varepsilon - \mathbb{1}_{\text{pass}})\} = \sum_{\text{all events}} \omega$$

where

$$\omega = \frac{\zeta}{\varepsilon - \zeta}(\varepsilon - \mathbb{1}_{\text{pass}}) \tag{5.5}$$

is the weight to be assigned to each event in the case of one FNP lepton in the event. The generalization of this formalism to higher dimensions with multiple objects will be covered next.

### 5.4.2 Dynamic matrix method

The one lepton case readily generalizes to events with more than one lepton in a formalism that can handle an arbitrary number of leptons in the event. The method should be applied event-by-event, effectively resulting into a weight being assigned to each event. The predicted yield of events with FNP leptons is simply the sum of weights. A general formula will be derived starting from the two

objects case then specific examples will be given to illustrate the application of the method.

If two objects are present in the event, the probabilites $\varepsilon/\zeta$ will depend on the kinematic properties of these objects. Typically the probabilies will vary as a function of $p_{\mathrm{T}}$ and $|\eta|$. For this reason, the probabilities will be different and will have an index to identify the object under study: $\varepsilon_i/\zeta_i$ where $i = 1, 2....$ An identity similar to Eq. 5.1 can be formed for two objects with a change in notation for simplicity:

$$\begin{pmatrix} N_{TT} \\ N_{TL} \\ N_{LT} \\ N_{LL} \end{pmatrix} = \Lambda \times \begin{pmatrix} N_{RR} \\ N_{RF} \\ N_{FR} \\ N_{FF} \end{pmatrix}, \tag{5.6}$$

where $(N_{RR}, N_{RF}, N_{FR}, N_{FF})$ are the number of events with respectively two real, one real plus one FNP (two terms), and two FNP leptons before applying tight cuts, respectively, and $(N_{TT}, N_{TL}, N_{LT}, N_{LL})$ are the observed number of events for which respectively both lepton pass the tight cut, only one of them (two terms), or both fail the tight cut, respectively.

$\Lambda$ is given by:

$$\Lambda = \begin{pmatrix} \varepsilon_1\varepsilon_2 & \varepsilon_1\zeta_2 & \zeta_1\varepsilon_2 & \zeta_1\zeta_2 \\ \varepsilon_1(1-\varepsilon_2) & \varepsilon_1(1-\zeta_2) & \zeta_1(1-\varepsilon_2) & \zeta_1(1-\zeta_2) \\ (1-\varepsilon_1)\varepsilon_2 & (1-\varepsilon_1)\zeta_2 & (1-\zeta_1)\varepsilon_2 & (1-\zeta_1)\zeta_2 \\ (1-\varepsilon_1)(1-\varepsilon_2) & (1-\varepsilon_1)(1-\zeta_2) & (1-\zeta_1)(1-\varepsilon_2) & (1-\zeta_1)(1-\zeta_2) \end{pmatrix}$$

which can also be written in terms of a Kronecker product in Eq. 5.6 to obtain:

$$\begin{pmatrix} N_{TT} \\ N_{TL} \\ N_{LT} \\ N_{LL} \end{pmatrix} = \begin{pmatrix} \varepsilon_1 & \zeta_1 \\ \bar{\varepsilon}_1 & \bar{\zeta}_1 \end{pmatrix} \bigotimes \begin{pmatrix} \varepsilon_2 & \zeta_2 \\ \bar{\varepsilon}_2 & \bar{\zeta}_2 \end{pmatrix} \begin{pmatrix} N_{RR} \\ N_{RF} \\ N_{FR} \\ N_{FF} \end{pmatrix} \tag{5.7}$$

To make the notation more compact, the set of 4 numbers $(N_{TT}, N_{TL}, N_{LT}, N_{LL})$ can be represented by a rank 2 tensor $\mathcal{T}_{\alpha_1\alpha_2}$ where $\alpha_i$ corresponds to one object that is either tight (T) or loose (L). Similarly the numbers $(N_{RR}, N_{RF}, N_{FR}, N_{FF})$ can be represented by $\mathcal{R}_{\alpha_1\alpha_2}$ where $\alpha_i$ corresponds to one object that is either real (R) or FNP (F). With this convention, the Kronecker product of Eq. 5.7 can be obtained by contracting each index $\alpha_i$ of the tensors $\mathcal{T}$ or $\mathcal{R}$ by the $2 \times 2$ matrix ${\phi_{i\beta_i}}^{\alpha_i}$:

$$\mathcal{T}_{\beta_1\beta_2} = {\phi_{1\beta_1}}^{\alpha_1} {\phi_{2\beta_2}}^{\alpha_2} \mathcal{R}_{\alpha_1\alpha_2}, \ \phi_i = \begin{pmatrix} \varepsilon_i & \zeta_i \\ \bar{\varepsilon}_i & \bar{\zeta}_i \end{pmatrix} \tag{5.8}$$

Following the same procedure as in the one object case, the matrix inversion of the $4\times4$ $\lambda$ matrix is simplified to a matrix inversion of the $2\times2$ $\phi$ matrices. The quantity of interest is the FNP lepton background that passes the tight selection criteria as in Eq. 5.4 which can be compactly written in the two objects case as:

$$\mathcal{T}^{\text{FNP}}_{\nu_1\nu_2} = {\phi_{\nu_1}}^{\mu_1} {\phi_{\nu_2}}^{\mu_2} \xi^{\beta_1\beta_2}_{\mu_1\mu_2} {\phi^{-1}}_{\beta_1}^{\alpha_1} {\phi^{-1}}_{\beta_2}^{\alpha_2} \mathcal{T}_{\alpha_1\alpha_2}. \tag{5.9}$$

The tensor $\xi$ encodes the component of tight and FNP lepton background. In the two objects case, $\xi$ needs to select the total background with at least one fake

lepton $N_F = N_{RF} + N_{FR} + N_{FF}$ that are also passing the tight selection criteria corresponding to the region with signal leptons. As a result, $\xi$ takes the form:

$$\xi = \begin{pmatrix} 0 & 0 & 0 & 0 \\ 0 & 1 & 0 & 0 \\ 0 & 0 & 1 & 0 \\ 0 & 0 & 0 & 1 \end{pmatrix}$$

To further illustrate, Eq. 5.9 can be written explicitely in the notation of Eq. 5.6 as:

$$N_{\text{FNP}}^{\text{signal}} = \begin{pmatrix} 0 & \varepsilon_1\zeta_2 & \zeta_1\varepsilon_2 & \zeta_1\zeta_2 \end{pmatrix} \Lambda^{-1} \begin{pmatrix} N_{TT} \\ N_{TL} \\ N_{LT} \\ N_{LL} \end{pmatrix}$$

The generalization of Eq. 5.9 from the two objects case to $m$ number of objects in the final state is straightforward:

$$\mathcal{T}^{\text{FNP}}_{\nu_1\cdots\nu_m} = \phi_{\nu_1}{}^{\mu_1}\cdots\phi_{\nu_m}{}^{\mu_m}\xi^{\beta_1\cdots\beta_m}_{\mu_1\cdots\mu_m}\phi^{-1}{}_{\beta_1}{}^{\alpha_1}\cdots\phi^{-1}{}_{\beta_m}{}^{\alpha_m}\mathcal{T}_{\alpha_1\cdots\alpha_m}. \tag{5.10}$$

The tensor $\xi$ is of the general form

$$\xi^{\beta_1\cdots\beta_m}_{\mu_1\cdots\mu_m} = \delta^{\beta_1}_{\mu_1}\cdots\delta^{\beta_m}_{\mu_m} h\left(\beta_1,\cdots,\beta_m,\nu_1,\cdots,\nu_m\right)$$

where the function $h$ can take values 0 or 1 based on the tight or loose configuration being computed which is encoded in the dependence on the indices $\nu_i$.

The application of the matrix method to multilepton final states comes with two specificities. Firstly, contributions of events with charge-flip electrons would bias a straightforward matrix method estimate (in particular for a final state formed by two leptons with same electric charge). This happens because the candidate-to-signal efficiency for such electrons is typically lower than for real electrons having a correctly-assigned charge. One therefore needs to subtract from $n_{\text{pass}}$ and $n_{\text{fail}}$ the estimated contributions from charge-flip. This can be performed by including as well events with pairs of opposite-sign candidate leptons in the matrix method estimate, but assigning them an extra weight corresponding to the charge-flip weight. Thanks (again) to the linearity of the matrix method with respect to $n_{\text{pass}}$ and $n_{\text{fail}}$, this weight-based procedure is completely equivalent (but more practical) to the aforementioned subtraction.

Secondly, the analytic expression of the matrix method event weight depends on the lepton multiplicity of the final state. This concerns events with three or more candidate leptons: one such event takes part both in the evaluation of the FNP lepton background for a selection with two signal leptons or a selection with three signal leptons, but with different weights[2]. Therefore, for a given event used as input to the matrix method, one should consider all possible leptons combinations, each with its own weight and its own set of kinematic variables. For example, a $e^+e^-\mu^+$ event is comptabilized in the background estimate both as an $e^+\mu^+$ event (with a weight w1) and as an $e^+e^-\mu^+$ event (with a weight $w_2 \neq w1$).

[2]This can appear for inclusive selections: for example an event with two signal leptons may or not contain additional candidate leptons, in a transparent way

### 5.4.3 Propagation of uncertainties

The two parameters ($\varepsilon$ and $\zeta$ respectively) can be measured in data, and depend on the flavor and kinematics of the involved leptons. Systematic uncertainties resulting from the measurement of these two parameters, and their extrapolation to the signal regions, can be propagated to uncertainties on the event weight through standard first-order approximations. The different sources of uncertainties should be tracked separately so that correlations of uncertainties across different events can be accounted for correctly. The resulting set of uncertainties on the cumulated event weights can be then added in quadrature to form the systematic uncertainty on the predicted FNP lepton background yield. The corresponding statistical uncertainty can be taken as the RMS of the event weights.

# Chapter 6

# Search for new physics in events with two same sign leptons or three leptons and jets

## 6.1 Introduction

As discussed in Chapter ??, supersymmetry (SUSY) is a theoretically favoured extension of the Standard Model (SM), which for each degree of freedom of the SM predicts another degree of freedom with a different spin. These degrees of freedom combine into physical superpartners of the SM particles: scalar partners of quarks and leptons (squarks ($\tilde{q}$) and sleptons), fermionic partners of gauge and Higgs bosons (gluinos ($\tilde{g}$), charginos ($\tilde{\chi}_i^{\pm}$, with $i$ = 1,2) and neutralinos ($\tilde{\chi}_i^0$ with $i$ = 1,2,3,4)), all with identical quantum numbers to their SM partners, except spin. If $R$-parity is conserved the lightest supersymmetric particle (LSP) is stable and is typically the lightest neutralino $\tilde{\chi}_1^0$which is a viable dark matter candidate.

As some of these particles are expected to be in the TeV-range, the discovery (or exclusion) of weak-scale SUSY is one of the highest physics priorities for the LHC. Both the ATLAS and CMS collaborations have carried out a vigorous search program for SUSY in various final states.

In this chapter, a detailed description will be given for the search for supersymmetric particles with an experimental signature involving multiple leptons in the final state. The search strategy will be covered along with the event selection procedure and the mechanisms by which the various backgrounds are estimated.

The results of the analysis will be interpretted in the context of simplified and popular supersymmetric models and also recast in terms of model independent limits.

In order to address the SM hierarchy problem with SUSY models , the masses of the partners of the gluons (gluinos $\tilde{g}$) and of the top quark chiral degrees of freedom (top squarks $\tilde{t}_L$ and $\tilde{t}_R$), and the partners of the bottom quark (sbottom) are expected to be in the TeVrange. The production cross sections for gluino pairs ($\tilde{g}\tilde{g}$), top–antitop squark pairs ($\tilde{t}_1\tilde{t}_1^*$) and bottom–antibottom squark pairs ($\tilde{b}_1\tilde{b}_1^*$) are relatively large which makes them a primary target for the early search program with the LHC data citeBorschensky:2014cia. The cascade decay of these SUSY particles may proceed via intermediate neutralinos $\tilde{\chi}^0_{2,3,4}$ or charginos $\tilde{\chi}^\pm_{1,2}$ that in turn lead to $W$, $Z$ or Higgs bosons, or to lepton superpartners (sleptons $\tilde{\ell}$) which will lead to isolated leptons and neutralinos $\tilde{\chi}^0_1$.

This searches focuses on final states with two leptons (electrons or muons) of the same electric charge (referred to as same-sign (SS) leptons) or three leptons (3L) in any charge combination or of same electric charge, jets and missing transverse momentum ($\vec{E}_{\mathrm{T}}^{\mathrm{miss}}$, whose magnitude is referred to as $E_{\mathrm{T}}^{\mathrm{miss}}$). Despite the penalty in signal yields due to the low branching ratio to SS/3L, the extreme background reduction achieved in this signature is a very good opportunity to discover new physics, particularly in scenarios with small mass differences between SUSY particles ("compressed scenarios"). This search is thus sensitive to a wide variety of models based on very different assumptions.

The results covered in the next sections use the full data collected in 2015 and

2016 by the ATLAS experiment in proton–proton ($pp$) collisions at a center-of-mass energy of $\sqrt{s} = 13\text{TeV}$, corresponding to a total integrated luminosity of 36.1 $\text{fb}^{-1}$.

It uses as signal benchmarks a few SUSY scenarios described in section 6.2. Observed data and predicted Standard Model yields are compared in a set of unbinned signal regions defined in section **??** ("cut and count"), and chosen to provide good sentivity to the signal benchmarks. The background prediction relies on Monte Carlo simulation of the relevant processes with prompt same-sign leptons and theoretical computations of their cross-sections (section **??**), and data-driven estimates of the contributions from processes with charge-flipped electrons (section **??**) or non-prompt or fake leptons (section **??**). The predictions are compared to observed data in a set of suitably chosen validation regions (section **??**) enriched in the different processes. Statistical interpretation of the observations in the signal regions is performed through the framework described in section **??**, which is also used by convenience to determine the total background yields in the signal regions, accounting for correlations between systematic uncertainties associated to the different background processes. These yields, compared to observed data, are reported in section **??**. In the absence of significant excess in observed data over the Standard Model prediction, exclusion limits are set on the masses of SUSY partners involved in the benchmark SUSY scenarios, and are presented in section **??**. Final conclusions are stated in section **??**.

## 6.2 Signal models

Final states with two same-sign leptons or three leptons and multiple jets are sensitive to a variety of new physics scenarios. In supersymmetric models in particular, such final states can be produced in the decays of heavy superpartners involving massive gauge bosons, sleptons or top quarks. Depending on the nature of the particles accompanying the leptons in the final states, a large variety of signatures can be obtained, notably in terms of the numbers of jets and $b$-tagged jets in the final state. We chose to illustrate the analysis versatility by evaluating its sensitivity to six $R$-parity-conserving (RPC) SUSY scenarios with the lightest neutralino $\tilde{\chi}_1^0$ as lightest and stable superpartner, featuring gluino, bottom squark or top squark pair production. The first scenarios studied focus on gluino pair production with decays into on-shell (Figure 6.1a) or off-shell (Figure 6.1b) top quarks, as well as on-shell light quarks. The latter are accompanied by a cascade decay involving a $\tilde{\chi}_1^\pm$ and a $\tilde{\chi}_2^0$ (Figure 6.1c) or a $\tilde{\chi}_2^0$ and light sleptons (Figure 6.1d). The other two scenarios target the direct production of third-generation squark pairs with subsequent electroweakino-mediated decays (Figures 6.1e and 6.1f). The former is characterized by final states with bottom squark pairs decaying to $t\bar{t}WW\tilde{\chi}_1^0\tilde{\chi}_1^0$. The latter, addressed here by looking at a final state with three same-sign leptons, is a model that could explain the excess seen in same-sign lepton signatures during Run 1 [**?**]. Finally, a full SUSY model with low fine-tuning, the non-universal Higgs model with two extra parameters (NUHM2) [**?**, **?**], is also considered. When the soft-SUSY-breaking electroweakino mass, $m_{1/2}$, is in

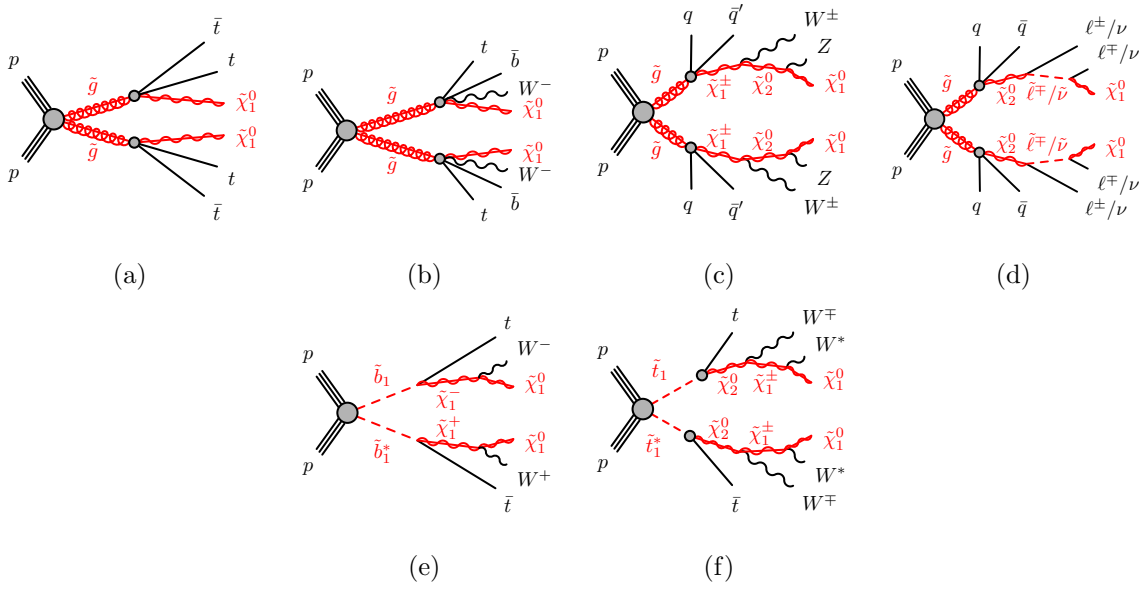


Figure 6.1: SUSY processes featuring gluino ((a), (b), (c), (d)) or third-generation squark ((e), (f)) pair production studied in this analysis. In Figure 6.1d, $\tilde{\ell} \equiv \tilde{e}, \tilde{\mu}, \tilde{\tau}$ and $\tilde{\nu} \equiv \tilde{\nu}_e, \tilde{\nu}_\mu, \tilde{\nu}_\tau$. In Figure 6.1f, the $W^*$ labels indicate largely off-shell $W$ bosons – the mass difference between $\tilde{\chi}_1^\pm$ and $\tilde{\chi}_1^0$ is around 1 GeV.

the range 300–800 GeV, the model mainly involves gluino pair production with gluinos decaying predominantely to $t\bar{t}\tilde{\chi}_1^0$ and $tb\tilde{\chi}_1^\pm$, giving rise to final states with two same-sign leptons and $E_{\mathrm{T}}^{\mathrm{miss}}$.

These scenarios were used as benchmarks to identify regions of the phase space where the analysis can bring particularly useful complementarity to other SUSY searches, and subsequently define our signal regions with a particular focus on these regions. In this section, the scenarios considered are presetend with details about the assumed superpartner masses and decay modes. Exclusion limits obtained prior to the work of the author will also be shown to highlight the improvement in reach after the current analysis.

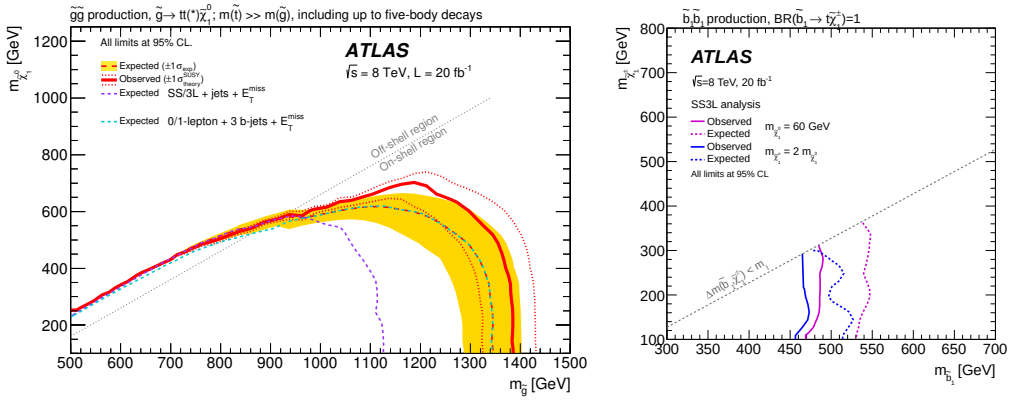


(a) (b)

Figure 6.2: Exclusion limits on the gluino-stop offshell (left) and direct sbottom (right) scenarios set by ATLAS with the 2012 dataset [**?**] prior to the author's work.

### 6.2.1 Gluino pair production with slepton-mediated two-step decay $\tilde{g} \to q\bar{q}\ell\bar{\ell}\tilde{\chi}_1^0$

This scenario (Fig. **??**) features gluino pair-production with two-step decays via neutralinos $\tilde{\chi}_2^0$ and sleptons, $\tilde{g} \to q\bar{q}'\tilde{\chi}_2^0 \to q\bar{q}'(\tilde{\ell}\ell/\tilde{\nu}\nu) \to q\bar{q}'(\ell\ell/\nu\nu)\tilde{\chi}_1^0$. The decays are mediated by generic heavy squarks, therefore the $b$-jet multiplicity in this scenario is low. The final state is made of charged leptons, four additional jets and invisible particles (neutrinos and neutralinos). The average jet multiplicity per event is the smallest among the four scenarios; another characteristic is the large fraction of events with several leptons, unlike the other scenarios that have a rather low acceptance due to the branching ratios of $W \to \ell\nu$ or $Z \to \ell\ell$. The exclusion limits obtained in run-1 (Fig. 6.3 right) show again that the SS/3L+jets final state is very competitive to probe those models. This scenario is used as as

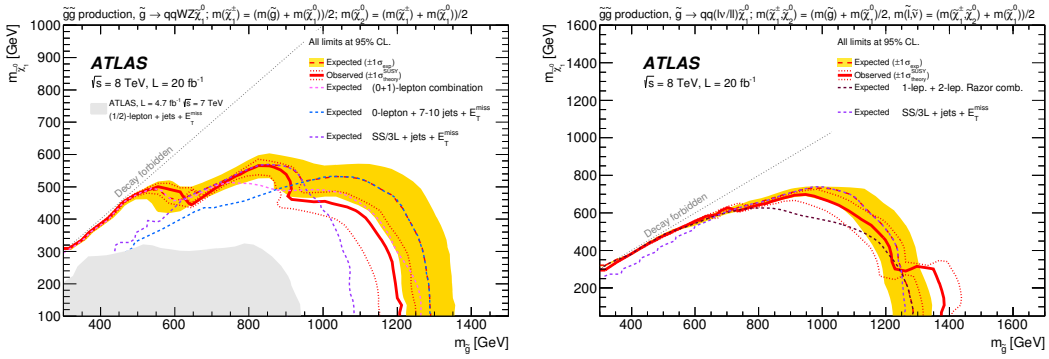


(a) (b)

Figure 6.3: Exclusion limits on scenarios featuring gluino pair production followed by two-step decays via heavy gauge bosons or sleptons, set by ATLAS with the 2012 dataset [**?**] prior to the author's work.

benchmark to define the signal regions with $\geq 3$ leptons and no $b$-jet.

The signal grid is built with variable gluino and $\tilde{\chi}_1^0$ masses; the $\tilde{\chi}_2^0$ mass is chosen half-way between the gluino and LSP masses, and the sleptons masses are also set equal and half-way between the $\tilde{\chi}_2^0$ and LSP masses. The $\tilde{\chi}_2^0$ may decay to any of the six "left-handed" sleptons ($\tilde{\ell}$, $\tilde{\nu}$) with equal probability. "Right-handed" sleptons are assumed heavy and do not participate to the decay.

### 6.2.2 Gluino pair production with gaugino-mediated two-step decay $\tilde{g} \to q\bar{q}'WZ\tilde{\chi}_1^0$

This scenario (Fig. **??**) features gluino pair-production with two-step decays via gauginos and $W$ and $Z$ bosons, $\tilde{g} \to q\bar{q}'\tilde{\chi}_1^\pm \to q\bar{q}'W\tilde{\chi}_2^0 \to q\bar{q}'WZ\tilde{\chi}_1^0$, mediated by generic heavy squarks of the first and second generations. The final state is made of two $W$ and two $Z$ bosons (possibly offshell), four additional jets and invisible

particles (neutrinos and neutralinos). This generally leads to events with large jet multiplicities and a fair branching ratio for dileptonic final states. The exclusion limits obtained in run-1 indeed illustrate the competitiveness of the SS/3L+jets search (Fig. 6.3 left) particularly the heavy-$\tilde{\chi}_1^0$ region of the phase space. This scenario is used as as benchmark to define the signal regions with many jets but none tagged as a $b$-jet.

The signal grid is built with variable gluino and $\tilde{\chi}_1^0$ masses, and the $\tilde{\chi}_1^\pm$ and $\tilde{\chi}_2^0$ masses are set such that the former lies half-way between the gluino and $\tilde{\chi}_1^0$ masses, and the latter half-way between $\tilde{\chi}_1^\pm$ and $\tilde{\chi}_1^0$ masses.

### 6.2.3 Sbottom pair production with one-step decay $\tilde{b}_1 \to t\tilde{\chi}_1^\pm$

In this scenario (Fig. **??**), bottom squarks are rather light and assumed to decay in a top quark and a chargino $\tilde{\chi}_1^\pm$, with a subsequent $\tilde{\chi}_1^\pm \to W^\pm\tilde{\chi}_1^0$ decay, providing complementarity to the mainstream search [**?**] which focuses on the channel $\tilde{b}_1 \to b\tilde{\chi}_1^0$. The final state resulting from the production of a $\tilde{b}_1\tilde{b}_1^*$ pair contains two top quarks, two $W$ bosons and two neutralinos. While this final state may lead to various experimental signatures, the model was considered in Run-1 [**?**] only by the same-sign leptons and jets search, leading to the exclusion limits presented in Fig. 6.2. Signal events typically contain one or two $b$-tagged jets, therefore this scenario is used as benchmark to define the signal regions with $\geq 1$ $b$-jet.

The model adopts a fixed chargino-neutralino mass difference of 100 GeV, therefore always allowing on-shell $W$ bosons in the $\tilde{\chi}_1^\pm \to W\tilde{\chi}_1^0$ decay [1] Only pair

[1] A different chargino mass assumption is adopted in the current work compared to the Run-1 paper [**?**]. Fig. 6.2 is shown for illustration only. The reduced chargino-neutralino mass gap in

production of the lightest sbottom is considered, followed by an exclusive decay in the aforementioned channel.

### 6.2.4 Gluino pair production with stop-mediated decay $\tilde{g} \to t\bar{t}\tilde{\chi}_1^0$

In this scenario inspired by naturalness arguments, gluinos are coupling preferentially to stops which are lighter than the other squarks. Gluinos are however considered lighter than stops, and decay directly into a $t\bar{t}\tilde{\chi}_1^0$ triplet via a virtual stop (Fig. **??**). The pair production of gluinos leads to a final state containing four top quarks and two neutralinos. This characteristic final state is accessible through various experimental signatures, which is why this model is commonly used as a benchmark to compare analyses sensitivities. The searches performed with Run-1 data [**?**], summarized in Fig. 6.2, showed that the same-sign leptons final state is competitive only at large neutralino mass. This region of the phase space is consequently given a particular attention in the choice of signal regions described further on. For instance, the region of phase-space with $\Delta m(\tilde{g}, \tilde{\chi}_1^0) < 2m_t$, where gluinos decay via one or two offshell top quarks, is only accessible for this analysis. In the signal samples referenced in this document, the mass of the lightest stop is fixed to 10 TeVand is mostly a $\widetilde{t}_R$ state. Only gluino pair production is considered, followed by an exclusive decay in the aforementioned channel. Signal events typically contain many $b$-tagged jets, therefore this scenario is used as benchmark to define the signal regions with $\geq 2$ $b$-jets.

the current analysis allows to study signal scenarios with heavy neutralinos, which were not considered previously.

### 6.2.5 $\tilde{t}_1\tilde{t}_1^*$ with "three-same-sign leptons" signature

Inspired by Ref. [**?**], a simplified model featuring a stop pair-production with two-step decays via a neutralino $\tilde{\chi}_2^0$ and a chargino $\tilde{\chi}_1^\pm$ is added in this version of the analysis, according to the decay illustrated on Fig. **??**:
$\tilde{t}_1 \to t\tilde{\chi}_2^0 \to t\tilde{\chi}_1^\pm W^\mp \to tW^\pm W^\mp \tilde{\chi}_1^0$.

This simplified model is a well-motivated representation of a pMSSM model. The lightest stop ($\tilde{t}_1$) is right-handed and $\tilde{\chi}_2^0$ is bino-like which leads to a large branching ratio in the decay $\tilde{t}_1 \to t\tilde{\chi}_2^0$. Furthermore, the decay $\tilde{\chi}_2^0 \to \tilde{\chi}_1^\pm W^\mp$ is also enhanced since $\tilde{\chi}_1^\pm$ is wino-like, as long as $\tilde{\chi}_1^\pm$ and $\tilde{\chi}_1^0$ are nearly mass degenerate and $m_{\tilde{\chi}_2^0} - m_{\tilde{\chi}_1^0} < m_H = 125$GeV to suppress the decay $\tilde{\chi}_2^0 \to \tilde{\chi}_1^0 + H$ (the decay $\tilde{\chi}_2^0 \to \tilde{\chi}_1^0 + Z$ is suppressed). By respecting these conditions and evading the bottom squark limit shown in Fig. **??**, c, we consider a one-dimensional grid with a $\tilde{t}_1$ mass varying between 550 GeVand 800 GeVwith a 50 GeVgap[2], a two body decay to an on-shell top quark and a $\tilde{\chi}_2^0$ which has a 100 GeVmass difference from $\tilde{\chi}_1^0$. The mass difference between the $\tilde{\chi}_1^\pm$ and $\tilde{\chi}_1^0$ is taken to be 500 MeVwhich is not excluded by the disappearing track analysis. In fact, this mass gap could easily be increased by introducing a small amount of higgsino mixing [**?**].

While the stop pair production is similar to the sbottom pair production in terms of kinematics, the stop pair production offers a unique topology that leads to three leptons of the same electric charge. This final state benefits from an extreme reduction of the SM background while maintaining a good signal acceptance which helps loosen the kinematic cuts to access a more compressed

[2]Only the points at $\tilde{t}_1$ mass of 550 GeV are available at the moment.

SUSY phase space. As a result, this scenario is complementary to the search for bottom squarks.

### 6.2.6 Non-Universal Higgs Models

In references [?, ?, ?], theorists studied a complete two-extra-parameter non-universal Higgs model (NUHM2) that can have low fine tuning (natural) and predicts final state signatures that allow large background rejection while retaining high signal efficiency. The NUHM2 model allows the soft SUSY breaking masses of the Higgs multiplets, $m_{H_u}$ and $m_{H_d}$, to be different from matter scalar masses ($m_0$) at the grand unification scale. The NUHM2 model is expected to form the effective theory for energies lower than $m_{GUT}$ resulting from SU(5) or general SU(10) grand unified theories. The scalar mass $m_0$, the soft SUSY breaking gaugino mass $m_{1/2}$, the pseudoscalar Higgs boson mass $m_A$, the trilinear SUSY breaking parameter $A_0$, the weak scale ratio of Higgs field vacuum expectation values $\tan\beta$, and the superpotential Higgs mass $\mu$ are the free parameters. Both $m_{1/2}$ and $\mu$ are varied while the other parameters are fixed to $m_0 = 5$ TeV, $A_0 = -1.6m_0$, $\tan\beta = 15$, $m_A = 1$ TeV, and sign($\mu$)>0. These parameter choices lead directly to a Higgs mass of 125 GeV in accord with experiment. In this "radiatively-driven natural" SUSY approach, the higgsino is required to have mass below 200-300 GeV, the stop to have a mass below $\sim$3 TeV, and the gluino below $\sim$4 TeV. Final state topologies that include MET, $W \to \ell\nu$ and that result in same-sign dileptons can be explored. Simulated NUHM2 signal samples with mass ($m_{1/2}$) values from 300-800 GeV and $\mu = 150$ GeV were generated. The gluino mass in this model is

| Decay | BR | Decay | BR |
|---|---|---|---|
| $t\bar{t}\chi_1^0$ | 0.13 | $tb\chi_1^\pm$ | 0.45 |
| $t\bar{t}\chi_2^0$ | 0.21 | $tb\chi_2^\pm$ | 0.04 |
| $t\bar{t}\chi_3^0$ | 0.13 | - | - |
| $t\bar{t}\chi_4^0$ | 0.02 | - | - |
| $t\bar{t}\chi_i^0$ | 0.49 | $tb\chi_i^\pm$ | 0.49 |

Table 6.1: The dominant gluino decay modes for $m_{1/2} = 400$ GeV for the NUHM2 model.

approximately $2.5 \times m_{1/2}$. Table 6.1 shows the branching ratios of the dominant gluino decay modes for $m_{1/2} = 400$ GeV.

### 6.2.7 Signal cross-sections and simulations

The signal processes are generated from leading order (LO) matrix elements with up to two extra partons (only one for the grid featuring slepton-mediated gluino decays), using the MADGRAPH v5.2.2.3 generator [**?**] interfaced to PYTHIA 8.186 [**?**] with the *ATLAS 14* tune [**?**] for the modelling of the SUSY decay chain, parton showering, hadronisation and the description of the underlying event. For the RPV models, MADGRAPH v5.2.3.3 and PYTHIA 8.210 [**?**] were used instead. Parton luminosities are provided by the NNPDF23LO [**?**] set of parton distribution functions. Jet-parton matching is realized following the CKKW-L prescription [**?**], with a matching scale set to one quarter of the pair-produced

Table 6.2: Signal cross-sections [pb] and related uncertainties [%] for scenarios featuring $\tilde{g}\tilde{g}$ (top table) or $\tilde{b}_1\tilde{b}_1^*$ (bottom table) production, as a function of the pair-produced superpartner mass, reproduced from Ref. [**?**].

| Gluino mass (GeV) | 500 | 550 | 600 | 650 | 700 |
|---|---|---|---|---|---|
| Cross section (pb) | $27.4 \pm 14\%$ | $15.6 \pm 14\%$ | $9.20 \pm 14\%$ | $5.60 \pm 14\%$ | $3.53 \pm 14\%$ |
| 750 | 800 | 850 | 900 | 950 | 1000 |
| $2.27 \pm 14\%$ | $1.49 \pm 15\%$ | $0.996 \pm 15\%$ | $0.677 \pm 16\%$ | $0.466 \pm 16\%$ | $0.325 \pm 17\%$ |
| 1050 | 1100 | 1150 | 1200 | 1250 | 1300 |
| $0.229 \pm 17\%$ | $0.163 \pm 18\%$ | $0.118 \pm 18\%$ | $0.0856 \pm 18\%$ | $0.0627 \pm 19\%$ | $0.0461 \pm 20\%$ |
| 1350 | 1400 | 1450 | 1500 | 1550 | 1600 |
| $0.0340 \pm 20\%$ | $0.0253 \pm 21\%$ | $0.0189 \pm 22\%$ | $0.0142 \pm 23\%$ | $0.0107 \pm 23\%$ | $0.00810 \pm 24\%$ |

| Sbottom mass (GeV) | 400 | 450 | 500 | 550 |
|---|---|---|---|---|
| Cross section (pb) | $1.84 \pm 14\%$ | $0.948 \pm 13\%$ | $0.518 \pm 13\%$ | $0.296 \pm 13\%$ |
| 600 | 650 | 700 | 750 | 800 |
| $0.175 \pm 13\%$ | $0.107 \pm 13\%$ | $0.0670 \pm 13\%$ | $0.0431 \pm 14\%$ | $0.0283 \pm 14\%$ |

superpartner mass.

The signal samples are normalised to the next-to-next-to-leading order cross-section from Ref. [**?**] including the resummation of soft gluon emission at next-to-next-to-leading-logarithmic accuracy (NLO+NLL), as detailed in Ref. [**?**]; some of these cross-sections are shown for illustration in Table 6.2. For the production of like-sign d-squark (RPV scenario), Prospino [**?**] is used to scale the samples to their NLO cross-section.

Cross-section uncertainties are also taken from Ref. [**?**] as well, and include contributions from varied normalization and factorization scales, as well as PDF

uncertainties. They typically vary between 15 and 25%. We do not consider any source of uncertainties on signal acceptance, experience having shown that these are generally smaller than the uncertainties on the inclusive production cross-section. [this is currently being verified for some cases]

The dataset IDs are listed in appendix **??**, Table **??**, and further details on simulation and reconstruction are provided in section **??**.

## 6.3 Data set and simulated event samples

The data used in this analysis were collected during 2015 and 2016 with a peak instantaneous luminosity of $L = 1.4 \times 10^{34}$ cm$^{-2}$s$^{-1}$. The mean number of $pp$ interactions per bunch crossing (pile-up) in the data set is 24. After the application of beam, detector and data-quality requirements, the integrated luminosity considered corresponds to 36.1 fb$^{-1}$. The uncertainty in the combined 2015+2016 integrated luminosity is 3.2%. It is derived, following a methodology similar to that detailed in Ref. [**?**], from a preliminary calibration of the luminosity scale using $x$–$y$ beam-separation scans performed in August 2015 and May 2016.

Monte Carlo (MC) simulated event samples are used to model the SUSY signals and to estimate the irreducible SM background with two same-sign and/or three "prompt" leptons. Prompt leptons are produced directly in the hard-scattering process, or in the subsequent decays of $W, Z, H$ bosons or prompt $\tau$ leptons. The reducible background, mainly arising from $t\bar{t}$ production, is estimated from the data as described in Section **??**. The MC samples were processed through a detailed

ATLAS detector simulation [?] based on GEANT4 [?] or a fast simulation using a parameterization of the calorimeter response and GEANT4 for the ID and MS [?]. To simulate the effects of additional *pp* collisions in the same and nearby bunch crossings, inelastic interactions were generated using the soft strong-interaction processes of PYTHIA 8.186 [?] with a set of tuned parameters referred to as the A2 tune [?] and the MSTW2008LO parton distribution function (PDF) [?]. These MC events were overlaid onto the simulated hard-scatter event and reweighted to match the pile-up conditions observed in the data. Table ?? presents, for all samples, the event generator, parton shower, cross-section normalization, PDF set and the set of tuned parameters for the modelling of the parton shower, hadronization and underlying event. In all MC samples, except those produced by the SHERPA generator, the EVTGEN v1.2.0 program [?] was used to model the properties of bottom and charm hadron decays.

The SUSY signals from Figure 6.1 are defined by an effective Lagrangian describing the interactions of a small number of new particles [?, ?, ?]. All SUSY particles not included in the decay of the pair-produced squarks and gluinos are effectively decoupled. These simplified models assume one production process and one decay channel with a 100% branching fraction. Apart from Figure ??, where events were generated with HERWIG ++ [?], all simplified models were generated from leading-order (LO) matrix elements with up to two extra partons in the matrix element (only up to one for the $\tilde{g} \to q\bar{q}(\ell\ell/\nu\nu)\tilde{\chi}_1^0$ model) using aMC@NLO 2.2.3 [?] interfaced to PYTHIA 8 with the A14 tune [?] for the modelling of the parton shower, hadronization and underlying event. Jet–parton

matching was realized following the CKKW-L prescription [**?**], with a matching scale set to one quarter of the pair-produced superpartner mass. All signal models were generated with prompt decays of the SUSY particles. Signal cross-sections were calculated at next-to-leading order (NLO) in the strong coupling constant, adding the resummation of soft-gluon emission at next-to-leading-logarithmic accuracy (NLO+NLL) [**?**, **?**, **?**, **?**, **?**], except for the RPV models of Figures **??** and **??** and the NUHM2 model where NLO cross-sections were used [**?**, **?**]. The nominal cross-sections and the uncertainties were taken from envelopes of cross-section predictions using different PDF sets and factorization and renormalization scales, as described in Refs. [**?**, **?**]. Typical pair-production cross-sections are: $4.7 \pm 1.2$ fb for gluinos with a mass of 1.7 TeV, $28 \pm 4$ fb for bottom squarks with a mass of 800 GeV, and $15.0 \pm 2.0$ fb for down squark-rights with a mass of 800 GeVand a gluino mass of 2.0 TeV.

The two dominant irreducible background processes are $t\bar{t}V$ (with $V$ being a $W$ or $Z/\gamma^*$ boson) and diboson production with final states of four charged leptons $\ell$,[3] three charged leptons and one neutrino, or two same-sign charged leptons and two neutrinos. The MC simulation samples for these are described in Refs. [**?**] and [**?**], respectively. For diboson production, the matrix elements contain the doubly resonant diboson processes and all other diagrams with four or six electroweak vertices, such as $W^{\pm}W^{\pm}jj$, with one ($W^{\pm}W^{\pm}jj$) or two ($WZ$, $ZZ$) extra partons. NLO cross-sections for $t\bar{t}W$, $t\bar{t}Z/\gamma^*(\rightarrow \ell\ell)$[4] and leptonic diboson

[3] All lepton flavours are included here and $\tau$ leptons subsequently decay leptonically or hadronically.

[4] This cross-section is computed using the configuration described in Refs. [**?**, **?**].

processes are respectively 600.8 fb [**?**], 124 fb and 6.0 pb [**?**]. The processes $t\bar{t}H$ and $4t$, with NLO cross-sections of 507.1 fb [**?**] and 9.2 fb [**?**] respectively, are also considered.

Other background processes, with small cross-sections and no significant contribution to any of the signal regions, are grouped into a category labelled "rare". This category contains $t\bar{t}WW$ and $t\bar{t}WZ$ events generated with no extra parton in the matrix element, and $tZ$, $tWZ$, $tt\bar{t}$, $WH$ and $ZH$ as well as triboson ($WWW$, $WWZ$, $WZZ$ and $ZZZ$) production with fully leptonic decays, leading to up to six charged leptons. The processes $WWW$, $WZZ$ and $ZZZ$ were generated at NLO with additional LO matrix elements for up to two extra partons, while $WWZ$ was generated at LO with up to two extra partons.

## 6.4 Event selection

## 6.5 Signal regions

## 6.6 Background estimation

## 6.7 Systematic uncertainties

## 6.8 Results and interpretation

## 6.9 Conclusion

A search for supersymmetry in events with two same-sign leptons or at least three leptons, multiple jets, $b$-jets and large $E_{\mathrm{T}}^{\mathrm{miss}}$ and/or large $m_{\mathrm{eff}}$ is presented. The analysis is performed with proton–proton collision data at $\sqrt{s} = 13$TeV collected in 2015 and 2016 with the ATLAS detector at the Large Hadron Collider corresponding to an integrated luminosity of 36.1 fb$^{-1}$. With no significant excess over the Standard Model prediction observed, results are interpreted in the framework of simplified models featuring gluino and squark production in $R$-parity-conserving and $R$-parity-violating scenarios. Lower limits on particle masses are derived at 95% confidence level. In the $\tilde{g}\tilde{g}$ simplified RPC models considered, gluinos with masses up to 1.85 TeV are excluded in scenarios with a light $\tilde{\chi}_1^0$. RPC models with bottom squark masses below 700 GeV are also excluded in a $\tilde{b}_1\tilde{b}_1^*$ simplified model with $\tilde{b}_1 \to tW^-\tilde{\chi}_1^0$ and a light $\tilde{\chi}_1^0$. In RPV scenarios, masses of down squark-rights are probed up to $m_{\tilde{d}_{\mathrm{R}}} \approx 500$ GeV. All

models with gluino masses below 1.3 TeV are excluded, greatly extending the previous exclusion limits. Model-independent limits on the cross-section of a possible signal contribution to the signal regions are set.

| Physics process | Event generator | Parton shower | Cross-section normalization | PDF set | Set of tuned parameters |
|---|---|---|---|---|---|
| Signal | | | | | |
| RPC | aMC@NLO 2.2.3 [?] | Pythia 8.186 [?] | NLO+NLL | NNPDF2.3LO [?] | A14 [?] |
| RPV except Fig. ?? | aMC@NLO 2.2.3 | Pythia 8.210 | or | NNPDF2.3LO | A14 |
| RPV Fig. ?? | Herwig 2.7.1 [?] | Herwig 2.7.1 | NLO-Prospino2 [?, ?, ?, ?, ?, ?] | CTEQ6L1 [?] | UEEE5 [?] |
| $t\bar{t}+X$ | | | | | |
| $t\bar{t}W$, $t\bar{t}Z/\gamma^*$ | aMC@NLO 2.2.2 | Pythia 8.186 | NLO [?] | NNPDF2.3LO | A14 |
| $t\bar{t}H$ | aMC@NLO 2.3.2 | Pythia 8.186 | NLO [?] | NNPDF2.3LO | A14 |
| $4t$ | aMC@NLO 2.2.2 | Pythia 8.186 | NLO [?] | NNPDF2.3LO | A14 |
| Diboson | | | | | |
| $ZZ$, $WZ$ | Sherpa 2.2.1 [?] | Sherpa 2.2.1 | NLO [?] | NNPDF2.3LO | Sherpa default |
| Other (inc. $W^{\pm}W^{\pm}$) | Sherpa 2.1.1 | Sherpa 2.1.1 | NLO [?] | CT10 [?] | Sherpa default |
| Rare | | | | | |
| $t\bar{t}WW$, $t\bar{t}WZ$ | aMC@NLO 2.2.2 | Pythia 8.186 | NLO [?] | NNPDF2.3LO | A14 |
| $tZ$, $tWZ$, $tt\bar{t}$ | aMC@NLO 2.2.2 | Pythia 8.186 | LO | NNPDF2.3LO | A14 |
| $WH$, $ZH$ | aMC@NLO 2.2.2 | Pythia 8.186 | NLO [?] | NNPDF2.3LO | A14 |
| Triboson | Sherpa 2.1.1 | Sherpa 2.1.1 | NLO [?] | CT10 | Sherpa default |

Table 6.3: Simulated signal and background event samples: the corresponding event generator, parton shower, cross-section normalization, PDF set and set of tuned parameters are shown for each sample. Because of their very small contribution to the signal-region background estimate, $t\bar{t}WW$, $t\bar{t}WZ$, $tZ$, $tWZ$, $tt\bar{t}$, $WH$, $ZH$ and triboson are summed and labelled "rare" in the following. NLO-Prospino2 refers to RPV down squark models of Figures **??** and **??**, as well as the NUHM2 model.

# Chapter 7

# Statistical Analysis

# Conclusion